Polarization-dependent angular distribution of the absorption behavior in Ytterbium-doped monoclinic LYB and LGB compounds

Wendwesen Gebremichael, Yannick Petit, S. Rouzet, Alexandre Fargues, Philippe Veber, Matias Velázquez, Veronique Jubera, Lionel Canioni, Inka Manek-Hönninger

Polarization-dependent angular distribution of the absorption behavior in ytterbium-doped monoclinic LYB and LGB compounds

W. Gebremichael[a,b], Y. Petit[c], S. Rouzet[b], A. Fargues[c], P.Veber[c], M. Velazquez[c], V. Jubera[c], L. Canioni[b], I. Manek-Hönninger[b]

[a]Amplitude Systèmes, Cité de la Photonique, 11 Avenue de Canteranne, 33600 Pessac, France; [b]CELIA University of Bordeaux-CNRS-CEA UMR5107, 351 cours de la Libération, 33405 Talence, France; [c] ICMCB-CNRS UPR9084, 87 Avenue du Dr Albert Schweitzer, 33600 Pessac, France

ABSTRACT

In this contribution we detail the full characterization of the anisotropy of the absorption properties of two different Yb-doped monoclinic borate compounds under polarized light. The studied crystals are $Li_6(Gd)_{0.75}Yb_{0.25}(BO_3)_3$ and $Li_6Y_{0.75}Yb_{0.25}(BO_3)_3$, respectively, grown by the Czochralski method. We focused on the study of their absorption at the zero line transition as a function of the polarization direction of the incident light for two different crystal cuts of each compound. We discuss the different Eigen frames that must be considered in these materials due to their monoclinic character, as well as the optimal crystal orientation for the considered absorption and the potential influences when used as laser materials.

Keywords: Monoclinic crystals, Angular distributions of spectroscopic properties, Lasers, Yb-doped crystals

1. INTRODUCTION

Ytterbium-doped crystals have proven to be attractive laser media and are used in industrial laser systems [1-6]. This is mainly due to the relatively small Stokes shift of these materials, which limits the heating effect during the laser process. Moreover, the absorption spectrum of the Ytterbium ion matches perfectly the emission wavelength of high power InGaAs laser diodes for pumping those laser crystals. Owing to the relatively large gain bandwidth depending on the host matrices Yb-doped crystals are suitable for ultrafast lasers and amplifiers down to the femtosecond regime.

Curiously, many of the commonly used materials, as e.g. double-tungstates, belong to the monoclinic system, such low symmetry being known to show non trivial optical specificities. Therefore, efficient use of such laser materials requires full spectral but angular characterization of their absorption and emission properties under polarized light. For most classes of crystals, measurements of these properties can be done along the dielectric frame axes which are described by the diagonalized 3-by-3 second-rank linear permittivity tensor. Given the anisotropic optical properties of monoclinic crystals, the general tensorial representation of the real and imaginary parts of dielectric permittivity shows that properties related to absorption or fluorescence should be considered separately and independently from the refractive properties, meaning that the real and imaginary parts of such low-symmetry linear permittivity tensor are diagonal in distinct frames [7][8].

In order to study these phenomena, we performed complete measurements of the absorption properties of two different Yb-doped monoclinic borate compounds under polarized light. The studied crystals are $Li_6(Gd)_{0.75}Yb_{0.25}(BO_3)_3$ and $Li_6Y_{0.75}Yb_{0.25}(BO_3)_3$, respectively [9]. Yb:LYB has already proven to be a suitable laser material, the optimum doping concentration had been determined, and first cw laser operation was previously reported [10]. Moreover, continuous wave, Q-switched and mode-locked laser operation has been demonstrated using an uncoated Yb:LYB crystal [11]. However, all these experiments were carried out without taking into account the monoclinic character of this compound. Therefore, we prepared Yb:LYB and Yb:LGB samples, very similar compositions, both monoclinic, and we focused on the study of their absorption at the zero line transition as a function of the polarization direction of the incident light for two different crystal cuts of each compound.

2. THEORETICAL BASICS

In the case of the three point groups of the monoclinic system, i.e. 2, m and 2/m [8] by assuming one of the axes of the dielectric frame (e.g. $\boldsymbol{y}$ axis) to be perpendicular to the mirror m or parallel to the two-fold axis 2, the general form of the complex permittivity tensor, $\hat{\bar{\bar{\varepsilon}}}_r(\omega)$ of the monoclinic crystals is described by a second-rank polar tensor with diagonal real part and with diagonal and two equal off-diagonal elements in a given tri-diagonal dielectric frame (x,y,z) [8].

$$\hat{\bar{\bar{\varepsilon}}}_r = \begin{bmatrix} \hat{\varepsilon}'_{r_{xx}} & 0 & \hat{\varepsilon}'_{r_{xz}} \\ 0 & \hat{\varepsilon}'_{r_{yy}} & 0 \\ \hat{\varepsilon}'_{r_{xz}} & 0 & \hat{\varepsilon}'_{r_{zz}} \end{bmatrix} = \begin{bmatrix} \varepsilon_{r_{xx}} & 0 & 0 \\ 0 & \varepsilon_{r_{yy}} & 0 \\ 0 & 0 & \varepsilon_{r_{zz}} \end{bmatrix} + j \begin{bmatrix} \varepsilon'_{r_{xx}} & 0 & \varepsilon'_{r_{xz}} \\ 0 & \varepsilon'_{r_{yy}} & 0 \\ \varepsilon'_{r_{xz}} & 0 & \varepsilon'_{r_{zz}} \end{bmatrix} \quad (1)$$

Equation (1) shows that we need three independent elements to fully represent the real part of the relative dielectric frame while there are four independent elements to fully represent the imaginary part of the relative dielectric frame. Similarly, given the imaginary frame (***x'***,***y'***,***z'***) in which the imaginary part is diagonalized, we need the values of three independent Eigen value parameters for such an imaginary frame while in this case the fourth independent parameter is the relative rotation of the ***x'z'***-plane around the ***y***=***y'*** axis with respect to the ***xz***-plane. In such a new absorption or emission Eigen frame, the imaginary part writes as a diagonal matrix [8]:

$$\bar{\bar{\varepsilon}}'_r = \begin{bmatrix} \varepsilon'_{r_{xx}} & 0 & \varepsilon'_{r_{xz}} \\ 0 & \varepsilon'_{r_{yy}} & 0 \\ \varepsilon'_{r_{xz}} & 0 & \varepsilon'_{r_{zz}} \end{bmatrix}_{dielectric} = \begin{bmatrix} \varepsilon'_{r_{x'x'}} & 0 & 0 \\ 0 & \varepsilon'_{r_{y'y'}} & 0 \\ 0 & 0 & \varepsilon'_{r_{z'z'}} \end{bmatrix}_{abs}, \theta_{abs} \quad (2)$$

It has been described that the imaginary part of the refractive index n' which governs absorption is related to the linear absorption coefficients for each of the two polarization Eigen-modes as:

$$\xi(\omega, \theta, \varphi) = 2\omega c^{-1} n'(\omega, \theta, \varphi) \quad (3)$$

where ξ[cm^{-1}] can be the absorption or fluorescence coefficient depending on the phenomenon considered during the experiment, c[cm/s] is the velocity of light in vacuum, and ω[1/s] is the circular frequency of light depending on the spherical coordinate angles (θ, φ) and the selected polarization Eigen-mode [8].

For the considered polarization Eigen-mode, the complex optical index, $\hat{n}(\omega, \theta, \varphi)$, is defined by:

$$\hat{n}(\omega, \theta, \varphi) = n(\omega, \theta, \varphi) + jn'(\omega, \theta, \varphi) \quad (4)$$

where $n(\omega, \theta, \varphi)$ and $n'(\omega, \theta, \varphi)$ represent the associated real and imaginary part of the refractive index, respectively.

3. EXPERIMENTS

This part describes the experimental approach followed to obtain the full absorption characteristics of the two borate type matrices of monoclinic crystals Yb:LGB and Yb:LYB, with molar doping rates of Yb^{3+}-ions of 22% and 26%, respectively [10]. Note that no specific spectral dispersion of the orientation of the dielectric frame orientation with respect to the crystallographic frame had been observed, so that the dielectric frame is considered as having a constant orientation in the red / near-IR range [8, 12].

3.1 Sample preparation

Given the crystallographic frame ***(a,b,c)*** in our borate crystals, the dielectric frame (***x,y,z***), as mentioned above, can be related to the crystallographic frame in such a way that the ***y***-dielectric axis is parallel to the ***b*** crystallographic axis, ***b//y*** since the monoclinic crystallographic axis ***b*** is perpendicular to the dielectric plane that contains the optical singularities corresponding to the umbilici of the refractive index surface, namely the *xz*-plane [8]. Therefore the ***y'***-axis of the absorption/fluorescence frame is also parallel to the ***y***-axis.

Based on this concept and the previous knowledge that ***y//b***, in order to access four independent terms, two groups of samples were prepared as illustrated in Table 1:

- **Group 1 (upper row in the table):** Crystals cut with the face perpendicular to the ***b*** crystallographic axis, *i.e.* direction of light propagation $\vec{k}$ or $-\vec{k}$ parallel to ***b//y***. The face is parallel to *xz*-plane in this case, giving direct access to the tensor elements ε_{xx} and ε_{zz}.
- **Group 2 (lower row in the table):** Crystals cut with the face parallel to the **b** crystallographic axis, *i.e.* direction of light propagation $\vec{k}$ or $-\vec{k}$ perpendicular to **b**//**y**. The **b**//**y axis** is parallel to the face, giving direct access to the tensor element ε_{yy} and indirect access to ε_{xz}.

Table 1. Crystallographic orientation of the studied LGB:Yb and LYB:Yb samples for the pump laser propagating towards the reader, upper row: group 1, lower row: group 2.

Direction of Cut	LGB:Yb 22%	LYB:Yb 26%	Properties accessed
Face ⊥ b (i.e. b // k or b//-k)	Sample 1 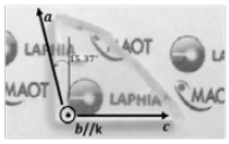	Sample 3 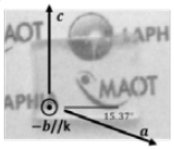	$\varepsilon'_{r_{xx}}$, $\varepsilon'_{r_{zz}}$
Face // b (a* or c* // k)	Sample 2 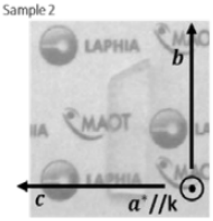	Sample 4 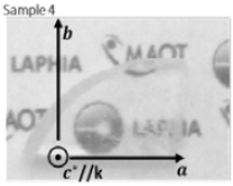	$\varepsilon'_{r_{yy}}$, $\varepsilon'_{r_{xz}}$

In order to correctly orientate the bulk crystals of the samples, its crystallographic orientation was determined using x-ray diffraction. Then the samples were cut and polished to optical quality.

3.2 Experimental setup

As described in Sec. 2, the imaginary part of the optical index governs absorption or fluorescence properties. Such an imaginary part is directly related to the linear absorption coefficient by equation (3), or the fluorescence counterpart coefficient, depending on the considered phenomenon. Here, the linear absorption coefficient measurements performed with the four Ytterbium-doped borate compound samples, as shown in Table 1, are explained. Specifically, the dependence of the effective measured linear absorption coefficient versus the incident linear polarization leads to a Malus law dependence, as given by equation (5). The maximum and minimum values are identified and estimated since they describe cases of light propagation with incident polarizations that correspond to an Eigen-mode polarization.

The aim of our experiment was to access the full angular distribution of the imaginary refractive index surfaces from the measurement of the absorption coefficient dependence with adapted non-redundant propagation directions and with the associated polarization Eigen-modes. The experimental setup for the absorption measurements is depicted in Figure 1.

The pump is a multimode diode laser emitting around 970 nm with a shift of ±5 nm depending on the temperature and the operating current. The linear absorption coefficient is highly dependent on the wavelength, and we have maximum absorption around 973 nm [9]. Therefore, a slight shift in the wavelength of the pump would lead to a significant change in the measured linear absorption coefficient emanating from the change in the wavelength as the absorption is strongly varying around the zero absorption line. Thus, we needed to systematically fix the wavelength of the pump at the zero phonon transition wavelength to ensure a relevant study of anisotropy of theses crystals for this specific transition.

The diode is fixed on a cooled heat sink that is temperature controlled by a chiller. For these experiments, the temperature was fixed at T = 28°C for an operation current of 5.2 A, corresponding to the absorption maximum of the laser diode emission for all four samples. This operation point was determined by measuring the transmitted power, with and without the crystal samples for varying input current values in steps of 0.5 A from 1 A to 4 A, and steps of 0.1 A from 4 A to 6 A, and observing the minimum transmittance. Then linear interpolation with steps of 0.01 A was done for the range 4 - 6 A. Note, that there was no difference for the LGB and LYB samples owing to the similarity of the two host matrices. As a result, we chose the same working point for both matrices, Yb:LGB and Yb:LYB corresponding to 5.2 A at T = 28°C.

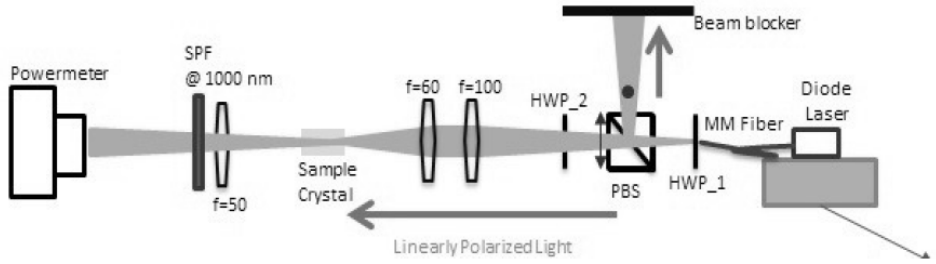

Figure 1. Setup for linear absorption coefficient measurement; f is in mm.

We used a combination of a half-wave plate, HWP1, and polarization beam splitter (PBS) to attenuate the laser power of the diode between ~0.3 W to ~2.4 W. Moreover, this ensures purely p-polarized light after the transmission by the PBS, which is crucial for this study. In order to measure the absorption coefficient dependence with the rotation of this linearly p-polarized light, we can either rotate the samples for a fixed p-polarized pump light or the p-polarized light for a fixed sample position using another half-wave plate HWP2. We used the second option in order to avoid influences by eventual local variations in crystal quality. In this case, the given angular rotation of the half wave plate, θ, leads to a 2θ rotation of the p-polarized light in the same direction.

4. RESULTS AND DISCUSSION

4.1 Determination of the linear absorption coefficient

We started the measurement of the absorption coefficient by measuring the transmittance of each sample, $T(\theta) = P_{sample}(\theta)/P_{no\_sample}(\theta)$ for the 360° rotation of HWP2 with steps of 10°. The resulting data points were fitted based on the formula below.

$$T(\theta) = T_{max}cos^2\left[2(\theta - \theta_{initial\_\lambda/2})\right] + T_{min}sin^2\left[2(\theta - \theta_{initial\_\lambda/2})\right] \quad (5)$$

The $\theta_{initial\_\lambda/2}$ represents the angle between the maximum transmittance value, T_{max}, and the neutral lines of HWP2. Great care was taken to properly manage (i) the potential offset between the physical orientation of the fast axis of HWP2 with respect to the mechanical graduations of its mount, as well as (ii) the specific position and associated orientation of each of the four crystals perpendicularly to the pump beam with respect to the absolute horizontal polarization (p-polarization) after the tunable attenuator made of HWP1 and the PBS.

Given the transmittance of the samples as in Equation (5), the absorption coefficient, α, can be calculated based on the measured thickness and on the Fresnel losses corrections from the previously determined refractive indices [9], as:

$$\alpha(\theta) = -\frac{1}{L}ln\frac{\left\{T_{max}cos^2\left[2(\theta - \theta_{initial\_\lambda/2})\right] + T_{min}sin^2\left[2(\theta - \theta_{initial\_\lambda/2})\right]\right\}}{T_{Fresnel}{}^2} \quad (6)$$

For the orientations of HWP2 at the angles $\theta_{initial\_\lambda/2}$ and $\theta_{initial\_\lambda/2} \pm 45°$, the measured absorption coefficient corresponds to α_{min} [cm^{-1}] and α_{max} [cm^{-1}], respectively. These values are associated to the propagation of individual Eigen-mode polarizations and are summarized in Table 2, where $\theta_{initial}$ corresponds to $2\theta_{initial\_\lambda/2}$.

Table 2. Minimum and maximum absorption coefficients and initial angle results of all the samples

Coefficients	**LGB**		**LYB**	
	Sample 1 (b//k)	Sample 2 (a*//k)	Sample 3 (-b//k)	Sample 4 (c*//k)
α_{min} (cm^{-1})	18.77±1.68	20.19±1.99	15.97±1.68	25.00±0.56
α_{max} (cm^{-1})	17.92±1.58	15.95±1.22	15.30±1.47	18.43±0.45
$\theta_{initial}$(°)	111.84±1.40	-0.63±3.98	17.07±3.21	92.25±1.40
Sample thickness L (cm)	0.176	0.137	0.139	0.181

4.2 Angular distributions of the imaginary parts of the optical index surfaces

From the minimum and maximum values of absorption coefficients for the four samples, it is possible to get the respective imaginary refractive index values that correspond to α_{min} and α_{max}, by applying equation (3). However, such four independent and non redundant measurements still need to be combined to determine the four independent tensor elements. They only give us specific information about the measured imaginary refractive index values on the principal dielectric planes perpendicular to the direction of propagation. Considering and carefully assigning these values, we can determine the imaginary refractive index surfaces on the three principal planes and we can obtain a good comparison between and among the real and imaginary principal axes on these planes.

For samples oriented with the faces perpendicular to the **b**-axis, a missing information is whether the measured T_{max} and T_{min}, or equivalently α_{min} and α_{max}, correspond either to the *x*- and *z*-axes, respectively, or to the opposite namely to the *z*- and x-axes. Such a determination is far from being trivial [7][12]. To overcome this undetermined situation, we successively applied these two possible hypotheses. As a result, for the samples where ***b*** or ***–b (y dielectric axis)*** is parallel or anti-parallel to the direction of light propagation, *i.e.* for the case of samples 1 and 3, there are two cases for the assignment of the x- and z- principal dielectric axes.

Case 1: Considering the case where the maximum values of the imaginary refractive indices are for an Eigen polarization mode along the x-axis of the dielectric frame.

Case 2: Considering the case where the maximum values of the imaginary refractive indices are for an Eigen polarization mode along the z-axis of the dielectric frame.

Once all the dielectric axes are assigned to the maximum and minimum values of the absorption coefficients, equation (3) can be used to calculate the corresponding imaginary parts of the optical indices associated to absorption along the considered polarization and propagation directions, these four measurements being respectively labeled n'_{xx}, n'_{yy}, n'_{zz} and $n'_{xz,exp}$. The n'_{xx}, n'_{yy} and n'_{zz} are in direct relationship with equation (2) expressed in the dielectric frame, with the equivalence given by equation (10). Then, the last measurement $n'_{xz,exp}$ can further lead to the estimation of the fourth off-diagonal tensor element n'_{xz} from equation (2), by applying equations (7) and (8) while considering the polar angle, θ_{xz}, that corresponds to the angle between the propagation direction with respect to the z-dielectric axis in the cases of samples 2 and 4. Given the initial angles, considering the crystallographic orientation and the propagation of the pump, such an angle θ_{xz} is determined for the two here-above detailed hypotheses as:

Case 1: $\theta_{xz} = \begin{cases} -21.86°/158.14° \pm 1.4° \ for\ Yb{:}\ LGB \\ 122.44°/-57.56° \pm 3.2° \ for\ Yb{:}\ LYB \end{cases}$

Case 2: $\theta_{xz} = \begin{cases} 68.15°/-111.85° \pm 1.4° \ for\ Yb{:}\ LGB \\ 32.44°/-147.56° \pm 3.2° \ for\ Yb{:}\ LYB \end{cases}$

Once we have all the real and imaginary index values to fill the right hand part of equation (9), we can determine the four independent parameters of the imaginary part of the permittivity tensor for the considered absorption transition, namely the left hand part of equation (9), by using the relationship (10) from reference [8].

Now it becomes possible to plot the angular distribution of the linear absorption coefficient in polarized light, or equivalently the imaginary part of the associated optical index for the zero phonon line absorption, leading to a double-layer imaginary index surface. The section of this surface on the principal planes gives "ordinary" and "extraordinary" complex optical indices [8]. The real part classically corresponds to the biaxial index surface with intersection in the dielectric planes as:

$$\begin{aligned} n^{e}_{xy}(\varphi) &= n_{zz} \text{ and } n^{o}_{xy}(\varphi) = \left[\frac{cos^2(\varphi)}{n^2_{yy}} + \frac{sin^2(\varphi)}{n^2_{xx}}\right]^{-1/2} \\ n^{o}_{yz}(\theta) &= n_{xx} \text{ and } n^{e}_{yz}(\theta) = \left[\frac{cos^2(\theta)}{n^2_{yy}} + \frac{sin^2(\theta)}{n^2_{xx}}\right]^{-1/2} \\ n^{o}_{xz}(\theta) &= n_{zz} \text{ and } n^{e}_{xz}(\theta) = \left[\frac{cos^2(\theta)}{n^2_{xx}} + \frac{sin^2(\theta)}{n^2_{zz}}\right]^{-1/2} \end{aligned} \tag{7}$$

Under the weak absorption approximation, the "ordinary" and "extraordinary" intersections of the imaginary part of the optical indices directly correspond to an "ordinary" and an "extraordinary" linear absorption coefficient with the following analytical angular dependence [8]:

$$\begin{aligned} n'^{o}_{xy}(\varphi) &= \frac{\varepsilon'_{r_{zz}}}{2n_{zz}} \text{ and } n'^{e}_{xy}(\varphi) = n^{e}_{xy}(\varphi)^3\left[\frac{\varepsilon'_{r_{yy}}cos^2(\varphi)}{2n^4_{yy}} + \frac{\varepsilon'_{r_{xx}}sin^2(\varphi)}{2n^4_{xx}}\right] \\ n'^{o}_{yz}(\theta) &= \frac{\varepsilon'_{r_{xx}}}{2n_{xx}} \text{ and } n'^{e}_{yz}(\theta) = n^{e}_{yz}(\theta)^3\left[\frac{\varepsilon'_{r_{yy}}cos^2(\theta)}{2n^4_{yy}} + \frac{\varepsilon'_{r_{zz}}sin^2(\theta)}{2n^4_{zz}}\right] \\ n'^{o}_{xz}(\theta) &= \frac{\varepsilon'_{r_{yy}}}{2n_{yy}} \text{ and } n'^{e}_{xz}(\theta) = n^{e}_{xz}(\theta)^3\left[\frac{\varepsilon'_{r_{xx}}cos^2(\theta)}{2n^4_{xx}} + \frac{\varepsilon'_{r_{zz}}sin^2(\theta)}{2n^4_{zz}} - \frac{\varepsilon'_{r_{xz}}sin(\theta)cos\,(\theta)}{n^2_{xx}n^2_{zz}}\right] \end{aligned} \tag{8}$$

where θ and φ are the polar and azimuthal angles, respectively, in the spherical coordinate system.

The imaginary part of relative dielectric permittivity can be given as:

$$\begin{bmatrix} \varepsilon'_{r_{xx}} & 0 & \varepsilon'_{r_{xz}} \\ 0 & \varepsilon'_{r_{yy}} & 0 \\ \varepsilon'_{r_{xz}} & 0 & \varepsilon'_{r_{zz}} \end{bmatrix}_{diel} = \begin{bmatrix} 2n'_{xx}n_{xx} & 0 & n'_{xz}(n_{xx}+n_{zz}) \\ 0 & 2n'_{yy}n_{yy} & 0 \\ n'_{xz}(n_{xx}+n_{zz}) & 0 & 2n'_{zz}n_{zz} \end{bmatrix}_{diel} \tag{9}$$

Thus we determine the off-diagonal element $\varepsilon'_{r_{xz}}$ by using equations (7) (8) and (9) as:

$$\varepsilon'_{r_{xz}} = \frac{n^2_{xx}n^2_{zz}}{sin(\theta_{xz})\,cos\,(\theta_{xz})}\left[\frac{\varepsilon'_{r_{xx}}cos^2(\theta_{xz})}{2n^4_{xx}} + \frac{\varepsilon'_{r_{zz}}sin^2(\theta_{xz})}{2n^4_{zz}} - n'^{e}_{xz}(\theta_{xz})\left[\frac{cos^2(\theta_{xz})}{n^2_{xx}} + \frac{sin^2(\theta_{xz})}{n^2_{zz}}\right]^{3/2}\right] \tag{10}$$

Once $\varepsilon'_{r_{xz}}$ is determined, we have the full information about both the real and imaginary parts of the complex permittivity, i.e. the full information about the anisotropy characterization of the absorption of our monoclinic crystal samples for the selected resonant transition. Table 3 shows the values of the imaginary parts of the optical indices determined from the absorption coefficient measurements of Yb:LGB and Yb:LYB samples with the dielectric x-axis being associated either to the maximum or to the minimum transmission values, as explained above, and labeled case 1 and case 2.

Table 3. Imaginary part of the optical indices expressed in the dielectric frame (left column) and in the absorption Eigen frames (right column). The angle $\theta_{rot}(°)$ describes the orientation of the absorption frame with respect to the dielectric frame, namely the rotation angle around the ***b***-axis (// to the *y*- and *y*-axes) to apply to pass from the dielectric frame to the absorption Eigen frame.

Imaginary Refractive Indices in dielectric frame		Imaginary Refractive Indices in absorption frame	
$\begin{bmatrix} n'_{xx} & 0 & n'_{xz} \\ 0 & n'_{yy} & 0 \\ n'_{xz} & 0 & n'_{zz_{zz}} \end{bmatrix}$	$\theta_{xz}(°)$	$\begin{bmatrix} n'_{xx} & 0 & 0 \\ 0 & n'_{yy} & 0 \\ 0 & 0 & n'_{zz} \end{bmatrix}$	$\theta_{rot}(°)$
Yb:LGB – case 1		Yb:LGB – case 1	
$\begin{bmatrix} 1.45 \pm 0.13 & 0 & 1.56 \pm 0.16 \\ 0 & 1.24 \pm 0.10 & 0 \\ 1.56 \pm 0.16 & 0 & 1.39 \pm 0.12 \end{bmatrix} \times 10^{-4}$	-21.86 /158.14 ± 1.4	$\begin{bmatrix} 1.24 \pm 0.08 & 0 & 0 \\ 0 & 1.24 \pm 0.10 & 0 \\ 0 & 0 & 1.60 \pm 0.17 \end{bmatrix} \times 10^{-4}$	51.22 ± 0.66
LGB – case 2		Yb:LGB – case 2	
$\begin{bmatrix} 1.39 \pm 0.12 & 0 & 1.56 \pm 0.16 \\ 0 & 1.24 \pm 0.10 & 0 \\ 1.56 \pm 0.16 & 0 & 1.45 \pm 0.13 \end{bmatrix} \times 10^{-4}$	68.15 /-111.85 ± 1.4	$\begin{bmatrix} 1.25 \pm 0.09 & 0 & 0 \\ 0 & 1.24 \pm 0.10 & 0 \\ 0 & 0 & 1.59 \pm 0.17 \end{bmatrix} \times 10^{-4}$	-40.28 ± 0.66
LYB – case 1		Yb:LYB – case 1	
$\begin{bmatrix} 1.24 \pm 0.13 & 0 & 1.94 \pm 0.04 \\ 0 & 1.43 \pm 0.03 & 0 \\ 1.94 \pm 0.04 & 0 & 1.19 \pm 0.11 \end{bmatrix} \times 10^{-4}$	122.44 /-57.56 ± 3.2	$\begin{bmatrix} 0.41 \pm 0.25 & 0 & 0 \\ 0 & 1.43 \pm 0.03 & 0 \\ 0 & 0 & 2.01 \pm 0.07 \end{bmatrix} \times 10^{-4}$	46.75 ± 0.54
LYB – case 2		Yb:LYB – case 2	
$\begin{bmatrix} 1.19 \pm 0.11 & 0 & 1.94 \pm 0.04 \\ 0 & 1.43 \pm 0.03 & 0 \\ 1.94 \pm 0.04 & 0 & 1.24 \pm 0.13 \end{bmatrix} \times 10^{-4}$	32.44 /-147.56 ± 3.2	$\begin{bmatrix} 0.39 \pm 0.25 & 0 & 0 \\ 0 & 1.43 \pm 0.03 & 0 \\ 0 & 0 & 2.04 \pm 0.08 \end{bmatrix} \times 10^{-4}$	-44.98 ± 0.52

Given these estimations of the four independent imaginary parameters, we can plot the imaginary part of the complex index surface in the xz plane, i.e. the intersections $n'^{o}_{xz}(\theta)$ and $n'^{e}_{xz}(\theta)$, as shown in Figure 2 for the two crystal matrices. As shown in the graphs a) to d), it is obviously verified that the angular positions of the minimal and maximal values of absorption depend in the dielectric frame on the considered hypothesis (cases 1 and 2). However, it is important to note that such angular positions of the minimal and maximal values of absorption are totally and univocally determined in the crystallographic frame, whatever the considered hypothesis among cases 1 and 2. Thus, such study allows for the absolute determination of the optical absorption direction in the crystallographic frame. Finally, as previously reported [8], the maximal/minimal absorption directions are out of the dielectric axes in the case of monoclinic samples.

To determine the orientation of the maximum and minimum imaginary parts of the optical indices with respect to the crystallographic orientation of the crystal samples, lets φ_{max} be the angle between the maximum absorption and the crystallographic axis **a**, and φ_{min} be the angle between the minimum absorption and the crystallographic axis **c**.

Table 4. Relative orientations of the maximum/minimum linear absorption coefficient with respect to the crystallographic axes of the LGB:Yb and LYB:Yb crystal samples considering two cases.

Angle(°)	LGB:Yb		LYB:Yb	
	Case 1	Case 2	Case 1	Case 2
φ_{max}(x',a)	32.3±2	33.8±2	91±4	92.8±2.5
φ_{min}(z',c)	16.9±2	18.4±2	75.7±4	77.4±4

As shown in Table 4, we have a rather good agreement of the specific directions of maximal/minimal absorption with respect to the crystallographic frame. This indicates that for any of the two considered hypotheses (cases 1 and 2), the maximum or minimum absorption crystal orientation will be univocally determined with respect to the crystallographic frame. The slight difference between the two cases may be because of the accumulated error for the numerical

approximations in the equations. Considering the above cases, the ratio of maximum to minimum of the imaginary part of the optical index gives 1.28±0.01 and 5±0.2 for LGB:Yb and LYB:Yb, respectively.

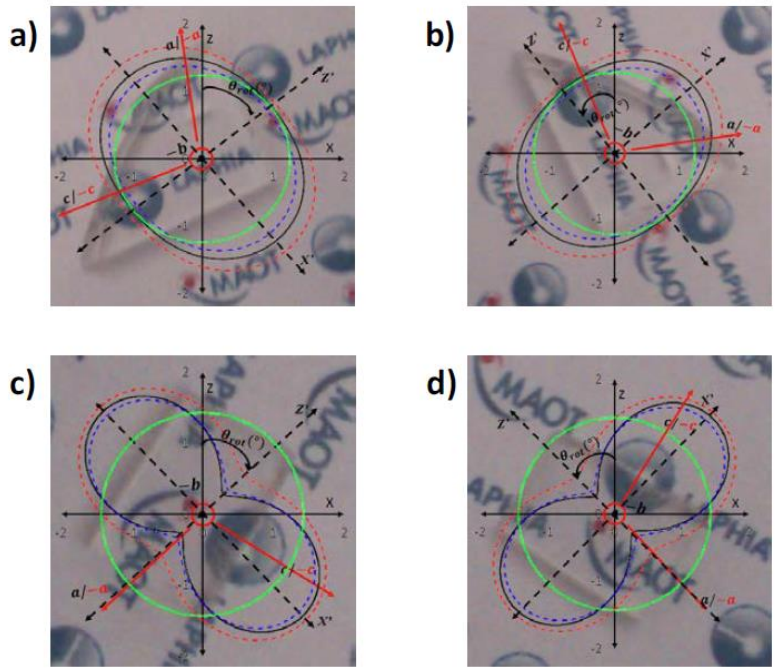

Figure 2. Intersections of the imaginary parts of the optical index surfaces, leading to ordinary (circular) and extraordinary (bi-lobal) distributions in the xz plane, related to the absorption anisotropy of both LGB:Yb and LYB:Yb. (a) LGB:Yb – case 1, (b) LGB:Yb – case 2, (c) LYB:Yb – case 1 and (d) LYB:Yb – case 2. The angle $\theta_{rot}(°)$ depicts the rotation of principal axes of the absorption frame, x' and z', with respect to the principal axes of the dielectric frame, x and z. Black solid lines: average values; orange and blue dashed lines: upper and lower error limit of sets of experiments.

5. CONCLUSION AND PERSPECTIVES

This study has led to the full determination of the four independent tensor elements of the imaginary part of the complex permittivity tensor, for the zero phonon line transition in absorption in two similar monoclinic borate matrix crystals similarly doped with Ytterbium ions. Although the matrices and the Ytterbium doping are similar, we show that the two samples show distinct anisotropies for the considered transition, with (i) different ratios between maximum and minimum absorptions (typically 1.3 against 5 for LGB:Yb and LYB:Yb) and (ii) different orientations of the optimal absorption directions (typically a remarkable difference of 60°).

This study confirms the universality of the optical specificities of monoclinic crystals, since such approach is based on highly-robust symmetry considerations [8], with (i) the existence of new Eigen frames related to each resonant transition in absorption and emission, these frames being different from each other and different from the dielectric frame and the crystallographic frame, and (ii) extremal absorption and emission cross sections out of the dielectric axes. This strengthens what has already been reported in different crystal matrices for different rare earth doping elements with laser properties [8, 13, 14].

This study suggests that further fundamental investigation is required to understand the origin of the orientation of these new Eigen absorption or emission frames and to model such a behavior, taking into account for each resonant transition the involved atomic orbital functions in the surrounding local crystal field in relationship to the local site symmetry, for different crystal matrices and rare earth ions.

ACKNOWLEDGMENT

This study has been carried out with financial support from the French State, managed by the French National Research Agency (ANR) in the frame of "the Investments for the future" Programme IdEx Bordeaux – LAPHIA (ANR-10-IDEX-03-02).

REFERENCES

[1] Nolte, S., Momma, C., Jacobs, H., Tünnermann, A., Chichkov, B.N., Wellegehausen, B., Welling, H., "Ablation of metals by ultrashort laser pulses," J. Opt. Soc. Am. B **14**, 2716 (1997).

[2] Loesel, F.H., Fischer, J.P., Götz, M.H., Horvath, C., Juhasz, T., Noack, F., Suhm, N., Bille, J.F., "Non-thermal ablation of neural tissue with femtosecond laser pulses," Appl. Phys. B **66**, 121 (1998).

[3] Limpert, J., Clausnitzer, T., Liem, A., Schreiber, T., Fuchs, H.J., Zellmer, H., Kley, E.B., Tünnermann, A., "High-average-power femtosecond fiber chirped-pulse amplification system," Opt. Lett. **28**, 1984 (2003).

[4] Hönninger, C., Courjaud, A., Rigail, P., Mottay, E., Delaigue, M., Deguil-Robin, N., Limpert, J., Manek-Hönninger, I., Salin, F., "0.5 µJ diode pumped femtosecond laser oscillator at 9 MHz," in OSA Trends in Optics and Photonics, Vol. 98, Advanced Solide-State Photonics, Optical Society of America, Washington, DC (2005).

[5] Killi, A., Steinmann, A., , A., Morgner, U., Lederer, M.J., Kopf, D., Fallnich, C., "High-peak-power pulses from a cavity-dumped Yb:$KY(WO_4)_2$ Oscillator," Opt. Lett. **30**, 1891 (2005).

[6] Innerhofer, E., Südmeyer, T., Brunner, F., Häring, R., Aschwanden, A., Paschotta, R., Hönninger, C., Kumkar, M., Keller, U., "60-W average power in 810-fs pulses from a thin-disk Yb:YAG laser," Opt. Lett. **28**, 367 (2003).

[7] Petit, Y., Boulanger, B., Segonds, P., Félix, C., Ménaert, B., Zaccaro, J., and Aka, G.,"Absorption and fluorescence anisotropies of monoclinic crystals: the case of Nd:YCOB," *Opt. Express*,. **16** (11), 7997–8002, 2008.

[8] Petit, Y., Joly, S., Segonds, P., and Boulanger, B., "Recent advances in monoclinic crystal optics," *Laser Photonics Rev.*, **7** (6), 920–937, 2013.

[9] Chavoutier, M., Ajrouche, H., Petit, Y., Garcia, A., Veber, P., Fargues, A., Viraphong, O., Jubera, V., Manek-Hönninger, I., Segonds, P., Debray, J., Ménaert, B., Rodriguez, V., and Adamietz, F., "Composition, geometry and polarization influences on spectroscopic properties of Yb-doped LLnB (Ln= Y, Gd) monoclinic crystals," SPIE Photonics West 2014-LASE Lasers Sources, vol. 8959, 89591M, 2014.

[10] Sablayrolles, J., Jubera, V., Delaigue, M., Manek-Hönninger, I., Chaminade, J.P., Hetjmanek, J., Decourt, R., Garcia, A., "Thermal properties and cw-laser operation of the ytterbium doped borate $Li_6Y(BO_3)_3$," Mater. Chem. Phys., **115**, 512 -515 (2009).

[11] Delaigue, M., Jubera, V., Sablayrolles, J., Chaminade, J.P., Garcia, A., Manek-Hönninger, I., "Mode-locked and Q-switched laser operation of the Yb-doped $Li_6Y(BO_3)_3$ crystal," Appl. Phys. B, **87**(4), 693-696 (2007).

[12] Traum, C., Inácio, P.L., Félix, C., Segonds, P., Peña, A., Debray, J., Boulanger, B., Petit, Y., Rytz, D., Montemezzani, G., Goldner, P., and Ferrier, A., "Direct measurement of the dielectric frame rotation of monoclinic crystals as a function of the wavelength," Optical Material Express **4**(1), 57-62 (2014).

[13] Brenier, A., Wu, Y., Zhang, J., Wu, Y., and Fu, P., "Laser properties of the diode-pumped Nd^{3+}-doped $La_2CaB_{10}O_{19}$ crystal," J. Appl. Phys. **108**, 093101 (2010).

[14] Brenier, A., "Polarization properties of lasing near an optical axis in the $KGd(WO_4)_2$:Nd biaxial crystal," Laser Phys. Lett. **11**, 115819 (2014).